Editors' Suggestion

Observation of Non-Abelian Thouless Pump

Oubo You,[1] Shanjun Liang,[2,*] Biye Xie,[1] Wenlong Gao,[3] Weimin Ye,[4] Jie Zhu,[5,6,*] and Shuang Zhang[1,7,†]
[1]Department of Physics, University of Hong Kong, Hong Kong, China
[2]Division of Science, Engineering and Health Studies, College of Professional and Continuing Education, Hong Kong Polytechnic University, Hong Kong, China
[3]Department of Physics, Paderborn University, Warburger Straße 100, 33098 Paderborn, Germany
[4]College of Optoelectronic Science and Engineering, National University of Defense Technology, Changsha, 410073, China
[5]Institute of Acoustics, School of Physics Science and Engineering, Tongji University, Shanghai 200092, China
[6]Department of Mechanical Engineering, Hong Kong Polytechnic University, Hong Kong, China
[7]Department of Electronic and Electrical Engineering, University of Hong Kong, Hong Kong, China

(Received 9 November 2021; revised 17 January 2022; accepted 16 May 2022; published 16 June 2022)

Thouless pump provides robust ways to realize quantized transport of waves and particles, and it casts the static 2D quantum Hall effect onto 1D dynamic systems where one of the momentum dimensions is replaced by the evolution time or path parameter. In the past few decades, various types of Abelian Thouless pump have been achieved theoretically and experimentally. However, the study of non-Abelian Thouless pump is scarce, which tells us that the order of two evolution loops with the same base point cannot be changed, and there has been no experimental observation of non-Abelian Thouless pump. Here we report the observation of a non-Abelian Thouless pump in coupled acoustic waveguide array. The non-Abelian property originates from the noncommutative combination of two different $\mathbb{Z}_3$ pump cycles that traverse across multiple band degeneracies in the parameter space in a three-band system. Moreover, we can pump a specific initial state to any state on any lattice site by applying these two $\mathbb{Z}_3$ pump cycles multiple times in a well-designed sequence. Our study paves the way for exploring and utilizing non-Abelian dynamical effects in classical wave systems and may offer different recipes for quantum walking, quantum optics, and quantum computation.

DOI: 10.1103/PhysRevLett.128.244302

Thouless pump is a one-dimensional dynamic topological effect that shares the same topological mechanism as the renowned two-dimensional Chern insulators, with one momentum dimension replaced by a time variant evolution parameter [1]. As a fundamental topological phenomenon, Thouless pump has been theoretically proposed [2–5] and experimentally realized [6–13] in various physical systems, such as electronics [2,6], cold atoms [3,7,8], photonics [4,9–11], acoustics [5,12], and mechanics [13]. In the past few decades, as part of the booming development in the exploration of various topological phases of matter, the concept of Thouless pump has been extended to many different topological systems, such as higher-order topological pump [14,15], disclination topological pump [16], charge pump in four-dimensional Hall effect [17,18], $\mathbb{Z}_2$ spin pump [19], Floquet-Thouless Energy pump [20], and fractional pump [21].

Non-Abelian physics is another important field that has been extensively explored for decades in both high energy physics and condensed matter physics [22,23]. Since Yang and Mills [22] introduced the non-Abelian gauge field to explain the strong interaction, the non-Abelian gauge theory has become a thriving field in theoretical physics. Later, Wu and Yang also introduced [24] the non-Abelian Aharonov-Bohm effect which has caught wide attention and has been synthetically achieved in classical wave systems [25]. Besides the non-Abelian gauge field [25–27], non-Abelian anyons and statistics for explaining the celebrated fractional quantum Hall effect [28] have also been extended to a classical wave system [29]. Despite the differences of these works, they all feature noncommutativity of operations, which take the form of matrices (or tensors), with a simple example being two rotations in three-dimensional space about x and y axes. Because of the matrix form of operation, the final pumped state of the system is different from the initial state by a $U(N > 1)$ matrix rather than a simple unitary complex number originating from its Abelian counterpart. This difference makes the non-Abelian physics far more complicated and richer than the Abelian counterpart, with examples including non-Abelian Berry curvature and Bloch oscillations [30–34], non-Abelian nodal links and quaternion topological charges [35–38], Young monopole and non-Abelian Wilson line [39,40], and linked Weyl surfaces [41,42]. In particular, the non-Abelian anyons are regarded as one of the promising ways for achieving fault-tolerant topological quantum computing [28].

In most of the previous studies, the evolution paths of the topological pumps were nondegenerate everywhere, and

hence the pumping operator between two different paths is always Abelian (i.e., they are commutative with each other). On the other hand, topological pump along paths traversing through band degeneracies has remained largely unexplored. Such pump is expected to go beyond the previous descriptions because the evolution operators are now expressed as matrices in which two pump paths can be potentially non-Abelian. In a very recent work [43], Thouless pump with a doubly degenerate two-band system was theoretically studied, which features a $U(2)$ gauge field with noncommutativity between different closed loops in the parameter space. However, no experimental observation of dynamic non-Abelian Thouless pump effects has been reported thus far.

In this work, we report observation of non-Abelian Thouless pump in 1D acoustic waveguide array systems. The non-Abelian property manifests itself through the transition among three interacting states [44] in the evolution paths. When the order of evolution paths is interchanged, the topological pump evolves the same initial state into different final pumped states, hence exhibiting non-Abelian characteristics.

Here, the implementation of non-Abelian Thouless pump is based on an array of acoustic waveguides with carefully tailored coupling configurations, as shown in Fig. 1(a). Each unit cell has a cross section [Fig. 1(b)] featuring the coupling between three rectangular waveguides (labeled w_1, w_2, and w_3) via interconnected narrow

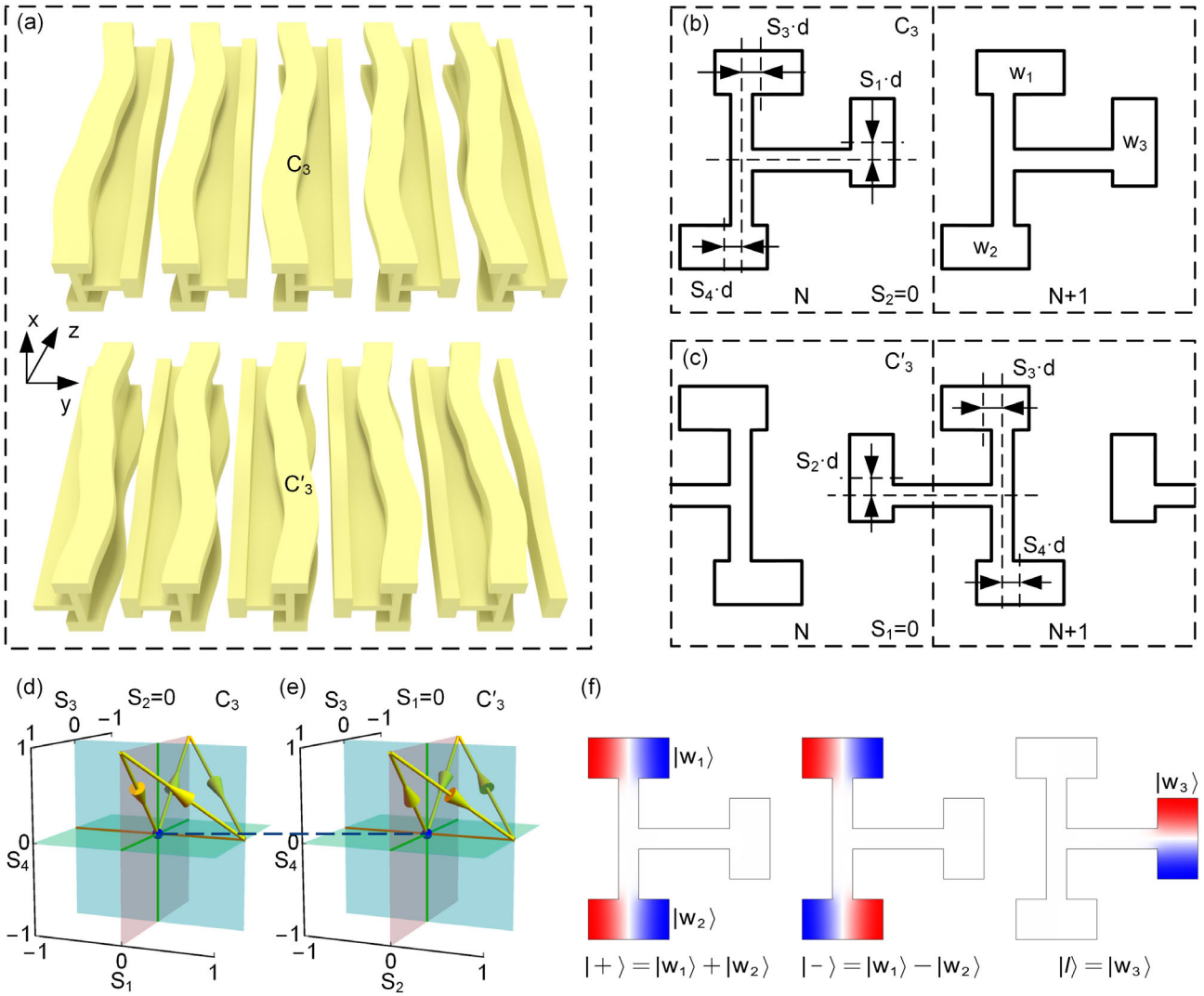

FIG. 1. Configurations of the acoustic waveguide arrays for the study of pumping. (a) Configurations of 1D periodic acoustic waveguide array for pumping loop C_3 and C_3'. (b),(c) Illustration of the geometric parameters of the cross section of the coupled waveguide array. The parameters S_i denote the offsets between the centers of the rectangular waveguides and T-shaped tube. (d) Illustration of the pumping loop C_3 (indicated by yellow arrows) in the parameter space, which resides in the $S_1S_3S_4$ subspace ($S_2 = 0$). (e) Illustration of the pumping loop C_3' in the parameter space, which resides in the $S_2S_3S_4$ subspace ($S_1 = 0$). The origins in (d) and (e) represent the same point, the origin in the full parameter space $S_1S_2S_3S_4$. (f) Field distribution for mode $|+\rangle$, $|-\rangle$, and $|l\rangle$.

tubes. Here only the p mode of the waveguide is considered, which has an antisymmetric field distribution along the long side of each waveguide. Hence, the offset of the interconnect tube from the center of the waveguide provides a means to control the sign and the amplitude of the coupling coefficient between them. Besides the intracell coupling, intercell coupling also exists between the neighboring unit cells through the interconnecting tubes, as shown in Fig. 1(c). Thus, considering both the intracell coupling and intercell coupling, the overall configuration is characterized by four normalized offset parameters, S_1, S_2, S_3, and S_4. The corresponding Hamiltonian for the configuration shown in Fig. 1(b) can be written as

$$\mathcal{H}(S_3, S_4, S_1) = \begin{pmatrix} \alpha_1 S_3^2 & \beta_1 S_3 S_4 & \beta_2 S_3 S_1 \\ \beta_1 S_3 S_4 & \alpha_1 S_4^2 & \beta_2 S_4 S_1 \\ \beta_2 S_3 S_1 & \beta_2 S_4 S_1 & \alpha_2 S_1^2 \end{pmatrix}. \quad (1)$$

More details, explanations, and validations of this Hamiltonian are provided in Supplemental Material, Sec. 2 [45].

Figure 1(a) shows the waveguide configurations corresponding to two different pumping loops, C_3 and C_3', which are the basic operations that will be combined in different sequences to construct the non-Abelian Thouless pump. The paths of C_3 and C_3' in the four-dimensional S_i parameter space are shown in Figs. 1(e) and 1(e), respectively. The C_3 loop is confined to the $S_1S_3S_4$ subspace; it starts from the origin $(0,0,0,0)$, and passes sequentially through $(0,0,-1,1)$, $(1,0,0,0)$, $(0,0,1,1)$, and finally returns back to the origin, and during the whole process, S_2 remains zero. On the other hand, the C_3' loop is confined to the $S_2S_3S_4$ subspace, and the path starts from the origin, and then sequentially passes through $(0,0,1,1)$, $(0,1,0,0)$, $(0,0,-1,1)$, and finally returns back to the origin, with S_1 remaining zero through the process. These two loops share the same base point located at the origin of the parameter space, where the three eigenstates are, respectively, the symmetric and antisymmetric modes formed by the p modes of the top and bottom (w_1 and w_2) waveguides (labeled $|+\rangle$ and $|-\rangle$, respectively), and the mode that is only localized in the linking waveguide w_3 ($|l\rangle$), as shown in Fig. 1(f). Because of the zero coupling between the neighboring group of connected waveguides at any given z, the energy bands are flat, so the isolated modes confined in each group can be regarded as maximumly localized Wannier functions. Hence the discretized shift of these modes after a complete cycle can be regarded as quantized transport in Thouless pump, which will be explained in detail later.

Because the propagation distance z is treated as time, the propagation constant k_z functions effectively as the energy in a 1D system. The operation of the C_3 loop to the initial states can be illustrated by the band evolution along the C_3 loop, as shown in Fig. 2(a). The transition between different states is enabled by the band crossings located at the origin and at (1, 0, 0, 0) in the parameter space. Starting from the origin in the parameter space, the three initial states $|+\rangle$ (enclosed by a blue square), $|-\rangle$ (enclosed by a green square), and $|l\rangle$ (enclosed by a red square) will evolve into $|l\rangle$, $|+\rangle$, and $|-\rangle$, respectively, after a single C_3 loop. Hence the three states form a permutation cycle under C_3 operation, as illustrated by Fig. 2(b). Note that all the transition occurs within the same unit cell, because S_2 remains zero along the C_3 loop; i.e., there is no coupling between neighboring unit cells during the evolution. Therefore, the projection of the operation on the evolved three-band subspace can be mathematically expressed as

$$C_3 = \sum_N (|l,N\rangle\langle +,N| + |-,N\rangle\langle l,N| + |+,N\rangle\langle -,N|), \quad (2)$$

with N denoting the site number. Based on Eq. (1), the original states will return back to themselves after three consecutive C_3 loops; i.e., the evolution loop C_3 represents a $\mathbb{Z}_3$ pump process. Similarly, the C_3' loop provides another permutation cycle between the three states but of opposite direction as C_3, as illustrated by Fig. 2(c). Importantly, C_3' operation involves the permutation among states $|+\rangle$ and $|-\rangle$ of one unit cell and $|l\rangle$ state in the unit cell to the left, and it can be mathematically expressed as

$$C_3' = \sum_N (|-,N\rangle\langle +,N| + |l,N-1\rangle \times \langle -,N| + |+,N\rangle\langle l,N-1|). \quad (3)$$

Equations (2) and (3) show that each single evolution is equivalent to a $\mathbb{Z}_3$ pump, and there is no lattice shift if the evolution path only consists of multiples of solely C_3 or C_3' because the $\mathbb{Z}_3$ topology leads to $C_3^3 = C_3'^3 = I$. However, if one combines these two different $\mathbb{Z}_3$ pump loops together, the lattice index in the expression can vary and the states can be pumped to the left or the right, or trapped, in an arbitrary manner. A unified description of the effects of these two pump loops is summarized in the map shown in Fig. 2(d). Based on this map, one can always construct a path to achieve pump from a state in a particular unit cell to any states in a different unit cell.

To elucidate such non-Abelian pump, we consider two synthetic $\mathbb{Z}_3$ pump paths, each consisting of three C_3 loops and one C_3' loop but arranged in different sequences, as indicated by the black solid and dotted lines in Fig. 2(d). For a given initial state $|+\rangle$, following the labeled sequence from 1 to 4, it will evolve into the final state of $|-\rangle$ for both paths, but the final state is pumped to the right for the path with sequence of $C_3C_3C_3'C_3$ [path 1, corresponding to the dashed line in Fig. 2(d)] and trapped for the other path with a sequence of $C_3'C_3C_3C_3$ (path 2, corresponding to the solid line). The simulation results on waveguide

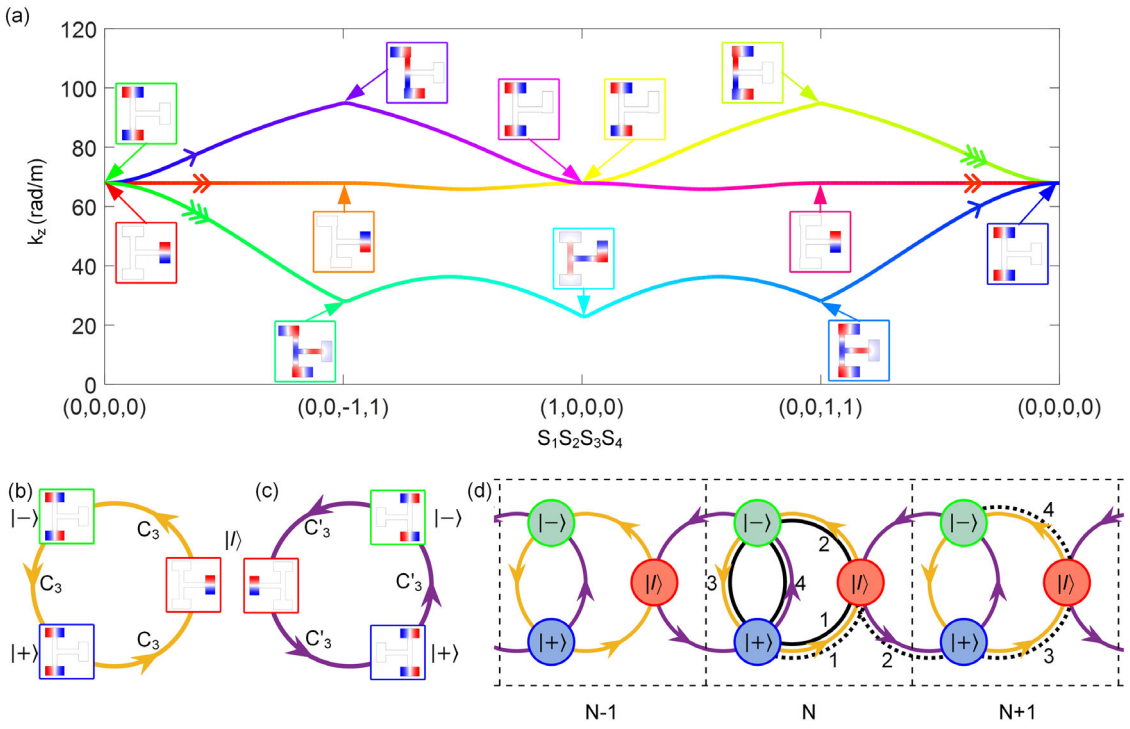

FIG. 2. Illustration of the $\mathbb{Z}_3$ pumping cycles and non-Abelian Thouless pump. (a) The band evolution along the C_3 loop at frequency 9500 Hz. The evolution directions are indicated by the arrows, and the corresponding eigenstates are provided along the evolution path. (b),(c) A concise description of the operation of C_3 and C_3'. (d) The combination of C_3 and C_3' on 1D periodic waveguides for constructing non-Abelian Thouless pumps. Two paths $C_3C_3C_3'C_3$ and $C_3'C_3C_3C_3$ applied at initial state $|+,N\rangle$ are indicated by dotted and solid black lines.

configurations corresponding to these two evolution paths are provided in Supplemental Material, Sec. 3, confirming the pump and trapping behaviors for path 1 and path 2, respectively [45].

As shown in Figs. 1(d) and 1(e), C_3 and C_3' each contain four line segments in the parameter space, and each line segment has an evolution length of $P/4$ with P denoting the total evolution length of the waveguide corresponding to C_3 or C_3'. The overall propagation length of the system for each path, consisting of 16 segments, would be very long, which hampers the experimental observations due to the significant intrinsic attenuation after a long path. In order to facilitate the experimental implementation, we employ a cut-and-join process, in which different locations of the waveguides where the field distributions are identical to each other are joined together, and the evolution path in between is omitted, as detailed in Supplemental Material, Sec. 4 [45]. By doing this, the length of the waveguide array is significantly reduced without affecting the pumping results. The final shortened configurations of the waveguide array each consist of two components L_1 and L_2, which, when joined together in different orders, leads to different pumping behaviors. The corresponding acoustic pressure distributions simulated at an excitation frequency of 9200 Hz for both configurations are shown in Fig. 3(a). It is shown that, despite the greatly shortened propagation length, the two pumping operations formed by the combination of L_1 and L_2 clearly exhibit the same pump behaviors as the original paths consisting of four C_3/C_3' loops—the state is shifted to the right for one configuration (L_2L_1), and trapped for the other configuration with the order of the two operations swapped (L_1L_2), hence a clear evidence of the non-Abelian pumping behavior.

In the experiment, the acoustic waveguide is a 3D-printed structure surrounded by a 5-mm-thick wall consisting of material Somos EvoLVe 128, which can be treated as a rigid boundary for the airborne sound wave traveling inside. At the input ports, a pair of out-of-phase tiny-size armature drivers is used to excite the p mode acoustic wave inside the rectangular waveguide. At the ends of the waveguide, porous absorptive cotton is used as the nonreflection boundary. In order to measure the evolution of the field along the propagation direction, an array of tiny ladder holes is drilled into the top and bottom sides of each waveguide. The holes are sealed by 3D-printed plugs to ensure air tightness and are only unplugged when being measured. Experimental results of the acoustic pressure distribution at the top of both samples are shown in Fig. 3(b) for the two configurations corresponding to L_2L_1 and L_1L_2, respectively. The measured results clearly show

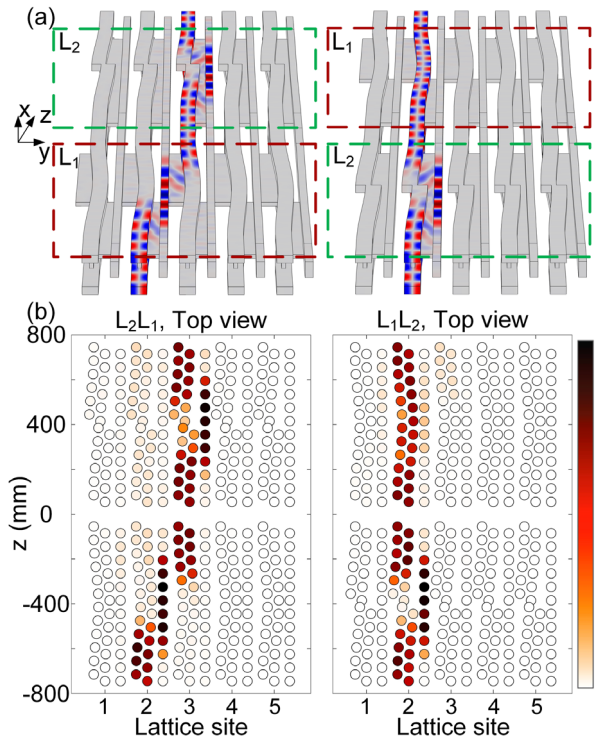

FIG. 3. Full wave simulation and measurement of the Thouless pumping. (a) The simulated acoustic pressure distribution along the paths L_2L_1 (left) and L_1L_2 (right), which are equivalent to the full evolution paths $C_3C_3C_3'C_3$ and $C_3'C_3C_3C_3$, respectively. The simulation clearly shows that the final state is pumped to the right for the paths L_2L_1, and trapped for L_1L_2. (b) The measured pressure at discrete locations along the path L_2L_1 and L_1L_2, which agree very well with the simulation results.

the expected non-Abelian pumping behaviors, which are in good agreement with the simulation results. More details of the experimental setup and data are given in Supplemental Material, Secs. 5–7 [45].

In summary, we have experimentally demonstrated non-Abelian Thouless pump in an acoustic waveguide system. Unlike the previous proposal in which the state evolution takes place in perfectly degenerate bands driven by non-Abelian Berry connections [43], the non-Abelian pump demonstrated here arises from a combination of different $\mathbb{Z}_3$ pump cycles enabled by band crossing in three connected bands. Hence, the non-Abelian holonomy (Wilczek-Zee phase) experiences an abrupt change at the band crossings, instead of being continuously accumulated along the path. Our study unequivocally demonstrates the non-Abelian characteristics of Thouless pump and paves the way for exploration of new physical phenomena and device applications based on non-Abelian dynamical effects in classical systems.

This work was supported by the Research Grants Council of Hong Kong (AoE/P-502/20, 17309021). O. Y., J. Z., and S. Z. initiated the project, O. Y. designed the structure, performed numerical simulations and analytical calculations, S. L. conducted the experiment, O. Y., S. L., B. X., W. G., W. Y., J. Z., and S. Z. participated in the analysis of the results, J. Z. and S. Z. supervised the project.O. Y. and S. L. contributed equally to this work. The authors declare no conflict of interest.

*jiezhu@tongji.edu.cn
†shuzhang@hku.hk

[1] D. J. Thouless, Phys. Rev. B **27**, 6083 (1983).
[2] Q. Niu, Phys. Rev. Lett. **64**, 1812 (1990).
[3] L. Wang, M. Troyer, and X. Dai, Phys. Rev. Lett. **111**, 026802 (2013).
[4] Y. G. Ke, X. Z. Qin, F. Mei, H. H. Zhong, Y. S. Kivshar, and C. Lee, Laser Photonics Rev. **10**, 995 (2016).
[5] Y. Long and J. Ren, J. Acoust. Soc. Am. **146**, 742 (2019).
[6] W. Ma, L. Zhou, Q. Zhang, M. Li, C. Cheng, J. Geng, X. Rong, F. Shi, J. Gong, and J. Du, Phys. Rev. Lett. **120**, 120501 (2018).
[7] M. Lohse, C. Schweizer, O. Zilberberg, M. Aidelsburger, and I. Bloch, Nat. Phys. **12**, 350 (2016).
[8] S. Nakajima, T. Tomita, S. Taie, T. Ichinose, H. Ozawa, L. Wang, M. Troyer, and Y. Takahashi, Nat. Phys. **12**, 296 (2016).
[9] M. Jurgensen, S. Mukherjee, and M. C. Rechtsman, Nature (London) **596**, 63 (2021).
[10] Z. Fedorova, H. Qiu, S. Linden, and J. Kroha, Nat. Commun. **11**, 3758 (2020).
[11] A. Cerjan, M. Wang, S. Huang, K. P. Chen, and M. C. Rechtsman, Light Sci. Appl. **9**, 178 (2020).
[12] W. Cheng, E. Prodan, and C. Prodan, Phys. Rev. Lett. **125**, 224301 (2020).
[13] I. H. Grinberg, M. Lin, C. Harris, W. A. Benalcazar, C. W. Peterson, T. L. Hughes, and G. Bahl, Nat. Commun. **11**, 974 (2020).
[14] W. A. Benalcazar, J. Noh, M. Wang, S. Huang, K. P. Chen, and M. C. Rechtsman, Phys. Rev. B **105**, 195129 (2022).
[15] H. Chen, H. Zhang, Q. Wu, Y. Huang, H. Nguyen, E. Prodan, X. Zhou, and G. Huang, Nat. Commun. **12**, 5028 (2021).
[16] B.-Y. Xie *et al.*, arXiv:2104.02852.
[17] M. Lohse, C. Schweizer, H. M. Price, O. Zilberberg, and I. Bloch, Nature (London) **553**, 55 (2018).
[18] O. Zilberberg, S. Huang, J. Guglielmon, M. Wang, K. P. Chen, Y. E. Kraus, and M. C. Rechtsman, Nature (London) **553**, 59 (2018).
[19] L. Fu and C. L. Kane, Phys. Rev. B **74**, 195312 (2006).
[20] M. H. Kolodrubetz, F. Nathan, S. Gazit, T. Morimoto, and J. E. Moore, Phys. Rev. Lett. **120**, 150601 (2018).
[21] L. Taddia, E. Cornfeld, D. Rossini, L. Mazza, E. Sela, and R. Fazio, Phys. Rev. Lett. **118**, 230402 (2017).
[22] C. N. Yang and R. L. Mills, Phys. Rev. **96**, 191 (1954).
[23] F. Wilczek and A. Zee, Phys. Rev. Lett. **52**, 2111 (1984).
[24] T. T. Wu and C. N. Yang, Phys. Rev. D **12**, 3845 (1975).
[25] Y. Yang, C. Peng, D. Zhu, H. Buljan, J. D. Joannopoulos, B. Zhen, and M. Soljacic, Science **365**, 1021 (2019).

[26] Y. Chen, R. Y. Zhang, Z. Xiong, Z. H. Hang, J. Li, J. Q. Shen, and C. T. Chan, Nat. Commun. **10**, 3125 (2019).
[27] P. Hauke, O. Tieleman, A. Celi, C. Ölschläger, J. Simonet, J. Struck, M. Weinberg, P. Windpassinger, K. Sengstock, M. Lewenstein, and A. Eckardt, Phys. Rev. Lett. **109**, 145301 (2012).
[28] C. Nayak, S. H. Simon, A. Stern, M. Freedman, and S. Das Sarma, Rev. Mod. Phys. **80**, 1083 (2008).
[29] T. Iadecola, T. Schuster, and C. Chamon, Phys. Rev. Lett. **117**, 073901 (2016).
[30] M. Di Liberto, N. Goldman, and G. Palumbo, Nat. Commun. **11**, 5942 (2020).
[31] T. Li, L. Duca, M. Reitter, F. Grusdt, E. Demler, M. Endres, M. Schleier-Smith, I. Bloch, and U. Schneider, Science **352**, 1094 (2016).
[32] J. Höller and A. Alexandradinata, Phys. Rev. B **98**, 024310 (2018).
[33] Y. Yan, S. L. Zhang, S. Choudhury, and Q. Zhou, Phys. Rev. Lett. **123**, 260405 (2019).
[34] S.-L. Zhang and Q. Zhou, Phys. Rev. A **95**, 061601 (2017).
[35] Q. Wu, A. A. Soluyanov, and T. Bzdusek, Science **365**, 1273 (2019).
[36] E. Yang, B. Yang, O. You, H.-C. Chan, P. Mao, Q. Guo, S. Ma, L. Xia, D. Fan, Y. Xiang, and S. Zhang, Phys. Rev. Lett. **125**, 033901 (2020).
[37] A. Tiwari and T. Bzdušek, Phys. Rev. B **101**, 195130 (2020).
[38] Q. Guo, T. Jiang, R. Y. Zhang, L. Zhang, Z. Q. Zhang, B. Yang, S. Zhang, and C. T. Chan, Nature (London) **594**, 195 (2021).
[39] S. Sugawa, F. Salces-Carcoba, Y. Yue, A. Putra, and I. B. Spielman, npj Quantum Inf. **7** (2021).
[40] S. Sugawa, F. Salces-Carcoba, A. R. Perry, Y. Yue, and I. B. Spielman, Science **360**, 1429 (2018).
[41] J.-Y. Chen, B. Lian, and S.-C. Zhang, Phys. Rev. B **100**, 075112 (2019).
[42] S. Ma, Y. Bi, Q. Guo, B. Yang, O. You, J. Feng, H. B. Sun, and S. Zhang, Science **373**, 572 (2021).
[43] V. Brosco, L. Pilozzi, R. Fazio, and C. Conti, Phys. Rev. A **103**, 063518 (2021).
[44] L. Michel and J. Zak, Phys. Rev. B **59**, 5998 (1999).
[45] See Supplemental Material at http://link.aps.org/supplemental/10.1103/PhysRevLett.128.244302 for geometric parameters, minimum Hamiltonian analysis, experimental setup and Chern number calculation of the waveguide system.